

Perpetual step-like restructuring of hippocampal circuit dynamics

Zheyang (Sam) Zheng¹, Roman Huszár^{1,2}, Thomas Hainmueller⁴, Marlene, Bartos⁵, Alex Williams^{1,2,6} and György Buzsáki^{2,3}

¹Center for Neural Science, New York University, New York, NY, USA.

²Neuroscience Institute, ³Department of Neurology, and ⁴Department of Psychiatry, NYU Grossman School of Medicine, New York University, New York, NY, USA.

⁵Institute for Physiology I, University of Freiburg, Medical Faculty, 79104 Freiburg, Germany

⁶Center for Computational Neuroscience, Flatiron Institute

Corresponding authors: Alex Williams (alex.h.williams@nyu.edu) or György Buzsáki (gyorgy.buzsaki@nyulangone.org)

Abstract

Representation of the environment by hippocampal populations is known to drift even within a familiar environment, which could reflect gradual changes in single cell activity or result from averaging across discrete switches of single neurons. Disambiguating these possibilities is crucial, as they each imply distinct mechanisms. Leveraging change point detection and model comparison, we found that CA1 population vectors decorrelated gradually within a session. In contrast, individual neurons exhibited predominantly step-like emergence and disappearance of place fields or sustained change in within-field firing. The changes were not restricted to particular parts of the maze or trials and did not require apparent behavioral changes. The same place fields emerged, disappeared, and reappeared across days, suggesting that the hippocampus reuses pre-existing assemblies, rather than forming new fields *de novo*. Our results suggest an internally-driven perpetual step-like reorganization of the neuronal assemblies.

Key words: representational drift, plasticity, place fields, quantal change, change point detection

35

36 Introduction

37 Balance between stability and flexibility is crucial for hippocampal function. Although
38 hippocampal place cells have long been assumed to be stable within the same environment^{1,2},
39 recent studies have found that population-wide representations become progressively dissimilar
40 as time lapses, without external perturbations³⁻⁵. These gradual changes, termed
41 “representational drift”, have timescales ranging from minutes to weeks. They have also been
42 reported in the piriform cortex⁶ and several neocortical areas⁷, although Jensen⁸ reported the lack
43 of drift in single neurons in the motor system.

44

45 While representational drift is often described as “gradual,” it is not yet clear whether the
46 underlying mechanism is “gradual” or “discrete”. This distinction is crucial for a mechanistic
47 understanding of the phenomenon. Hebbian spike-timing-dependent plasticity^{9,10} is expected to
48 change synaptic strength over many repetitions, thus gradually. On the other hand, behavioral
49 time scale synaptic plasticity¹¹⁻¹⁵ (BTSP) provides a mechanism for abrupt changes in neural
50 firing rate. Intracellular and imaging experiments *in vivo* have demonstrated that spontaneously
51 emerging ON fields often coincide with dendritic “plateau potentials” in CA1 pyramidal
52 neurons, attributed to the temporal coordination of their entorhinal and CA3 inputs^{12,16}. Thus,
53 representational drift in the hippocampus could conceivably consist of either gradual or discrete
54 changes in single-neuron activity patterns.

55

56 Studies of BTSP focus on the emergence of place fields (also translocation, i.e. emergence in one
57 and abolishment in another field, see Milstein et al.¹⁴) but not disappearance. Furthermore, it is
58 unclear whether neurons exhibit other forms of spontaneous abrupt changes, such as up or down-
59 modulation of firing rate (or “rate remapping”^{17,18}). The apparent lack of evidence could be due
60 to difficulties in detecting abrupt changes. The emergence of place fields is relatively well-
61 defined and can be detected by looking at when the within-field activity goes above
62 thresholds^{15,19}. Similarly, rate remapping is often induced by changing some experimental
63 condition (e.g., the wall color of the maze) and studied in a trial-averaged fashion^{17,18}. On the
64 other hand, spontaneous rate remapping is difficult to study without an unsupervised method for
65 detecting abrupt and sustained changes on a single trial level.

66

67 We developed a statistical framework that allows us to detect, determine, and link the type of
68 changes occurring on the single cell and population level. By analyzing datasets of large
69 simultaneous recordings of the CA1 pyramidal neurons, we show that population vectors of the
70 CA1 pyramidal cells are decorrelated as a function of elapsed trials gradually, akin to the gradual
71 drift view. In contrast, changes at the individual place cell level are better characterized by step-
72 like emergence and disappearance of place fields or steep changes in within-field firing, which
73 we call “switching.” We found that although spatial position, trial number, and novelty may
74 modulate the probability of place field turnover, switching can happen on every trial and in all
75 parts of the test environment without apparent behavioral changes. Switching is not a single-cell
76 property: neurons with multiple place fields can sustain stability in one field and change in
77 another field, and neurons with switching fields in one environment may remain stable in
78 another. Instead, switching appears to be driven by circuit dynamics, as place fields co-switch
79 together on the same trial more than expected by chance. Finally, the spontaneous emergence of
80 place fields on one day does not mean a *de novo* formation of a place field, but rather a “reuse”

81 of preexisting assemblies, as emerging and disappearing fields on one day could
82 preexist/reappear on the previous/next day. These findings bridge together single cell and
83 population features—the step-like and gradual views—and illustrate that preexisting cell
84 assembly blocks continuously reorganize themselves without external perturbations.

85

86

87

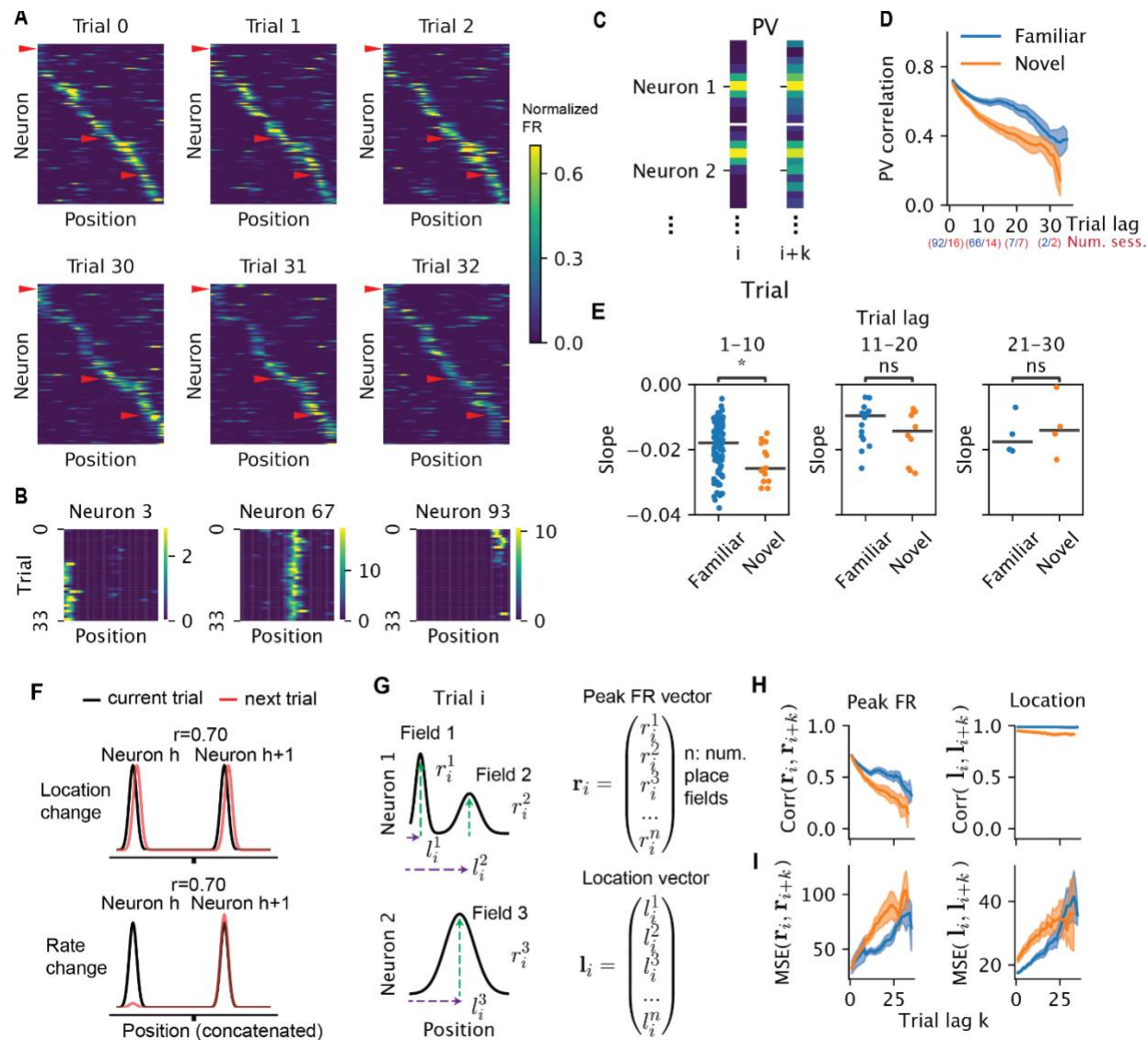
88 **Results**

89 We examined the stability of single units and populations of hippocampal CA1 pyramidal cells
90 while mice performed a spontaneous alternation task in a figure-8 maze either in a familiar or
91 novel environment²⁰ (schematics in Fig. 4K; see Method details). For multiple-day comparisons,
92 CA1 neurons detected by two-photon imaging were used as mice traversed a 1D virtual
93 hallway²¹.

94 **Within-session representational drift is driven by discrete switching of place fields**

95 As animals traversed the figure-8 maze, the dorsal CA1 population activity exhibited largely
96 similar sequential firing over the entire session (Fig. 1A; place cells with place fields¹). Yet, a
97 subset of neurons changed their firing rates substantially from the beginning to the end of the
98 session (Fig. 1B). To relate our initial observations to previous reports, we first analyzed the
99 correlation between population vectors (PVs) as a function of trial lag. The PVs are constructed
100 by concatenating the rate map of all place cells on a given trial (Fig. 1C). The correlation
101 decreased as a function of the lag between trials, suggesting drift within both the familiar and
102 novel environment (Fig. 1D). Linear regression analysis revealed that drift was significantly
103 faster in novel environments (larger negative slope) within the first 1-10 trial lags, but we failed
104 to detect any significant difference between novel and familiar environments over a range of 11-
105 20 or 21-30 trial lags (Fig. 1E). Thus, our analysis supports the idea that novelty destabilizes the
106 network^{15,22,23}, but also highlights a surprising degree of spontaneous drift that persists in
107 familiar environments.

108



109

110

11

Figure 1. Stability and change of single units and population activity. A) Population ratemaps of hippocampal place cells during early and late trials. Place cells were sorted by the peak of the place fields on trial 0 (when there were multiple fields, we used the fields with the largest within-field peak firing rates). Only place cells with spatial information larger than 1 bit/spike are displayed here for the ease of visualization; $n = 114$ out of 264 place cells for one direction of turn in the figure-8 maze). Color represents normalized firing rate. B) Ratemaps of 3 example neurons, marked by red arrowheads in A, showing place field emergence (left), stable firing (middle), and place field disappearance (right). C) Schematic for constructing the population vectors (PV) in D. The ratemaps for all neurons were concatenated on a given trial to form a PV. The Pearson correlation between PVs from a pair of trials was computed. All trial pairs with lag k were averaged to produce the mean PV correlation per trial lag. D) Population ratemap correlations as a function of trial lag (only place cells are included). Blue and orange correspond to familiar and novel sessions, respectively. Shaded area corresponds to 95 confidence interval, where each data point is the correlation

112

113 between two trials within one session. The number of included sessions for blocks of trials are indicated in
114 parentheses. E) Comparing the slope of PV correlation decay between familiar and novel environment in
115 three ranges of trial lags. Trial lag 1-10, N=106, Wilcoxon rank sum test, $p=0.02$, Cohen's $d = 0.58$; trial lag
116 11-20, N=26, $p=0.3$, Cohen's $d = 0.54$; trial lag 21-30, N=8, $p=0.68$, Cohen's $d=-0.35$. Stars indicating the
117 significance level for all figures (*, $0.01 < p \leq 0.05$; **, $0.001 < p \leq 0.01$, ***, $0.0001 < p \leq 0.001$; ****,
118 $p \leq 0.0001$). F) Schematics of different hypothetical mechanisms inducing a population level decorrelation.
119 Each Gaussian bump represents the tuning curve of one place cell. The Pearson correlation r is taken
120 between the black (current trial) and red (next trial) curves. G) Schematics for how the within-field peak
121 firing rate vector and place field location vector were constructed in H and I. H) Correlation of within-field
122 peak population firing rate (left) and peak location (right) of place cells as a function of trial lag. I) Similar
123 to E, but instead of correlation, the normalized squared Euclidean distance (equivalent to mean squared
124 error, MSE) is shown as a function of trial lags.
125

126

127 In principle, representational drift could be driven by a change in place field location or by a
128 change in the firing rate within the field, among other possibilities (Fig. 1F). We found the vector
129 of the peak firing rate of all place fields decorrelated as a function of trial lag, whereas the vector
130 of the place field locations remained stable (Fig. 1G-H). We emphasize though that the lack of
131 decorrelation does not mean the field locations do not change as a function of trial. In fact, the
132 average squared Euclidean distance as a function of trial lag increased significantly (Fig. 1I). We
133 focused on the decorrelation due to changes in firing rate for the rest of this paper.
134

135 The decorrelation of the population vectors could arise from either a gradual change (as implied
136 by the term “drift”^{3,4}) or a relatively sudden (“quantal”) jump¹¹ at the single cell level. By
137 qualitative inspection, we observed discrete and sustained changes in the within-field firing rates
138 (“quantal” change; Fig 2A,B). We refer to such step-like increases/decreases in firing rates, as
139 “switching ON/OFF” fields. To investigate switching quantitatively, we leveraged a change-
140 point detection model to fit a piecewise constant function to the peak within-field firing rates
141 across trials. The trials at which these step functions change values are determined to be change
142 points²⁴ (see Methods). To select the numbers of change points objectively, we compared the
143 observed fit to models fit on shuffled data where trial order was randomly permuted (Fig. 2C).
144 To rule out changes that were too small, we required change points to result in at least a 40%
145 change in firing rate (relative to the maximum). This restriction only ruled out 7% of the putative
146 switching fields (n = 212/3184).
147

148 Fig. 2A,B shows examples of switching ON and switching OFF fields. Importantly, the
149 switching does not only include a sudden appearance or disappearance of place fields, but also
150 drastic changes in firing rates of existing fields (see examples in Suppl. Fig. 7C). Overall, 19%
151 (2310/12311) of the place fields showed significant switching (14% ON, 9% OFF) in the

152 familiar environment (Fig. 2D) and 31% (662/2127, 25% ON, 18% OFF) in the novel
153 environment (Fig 2D), echoing the finding of higher rate of BTSP in novel environments ¹⁵.
154 Furthermore, a subgroup of animals exposed to both familiar and novel environments had less
155 training than the animals exposed to only the familiar environment. These animals had higher
156 fractions of switching fields (“Familiar” in Fig. 2E) than the “Familiar only” animals. Thus,
157 novelty seemed to destabilize the network in a graded way.

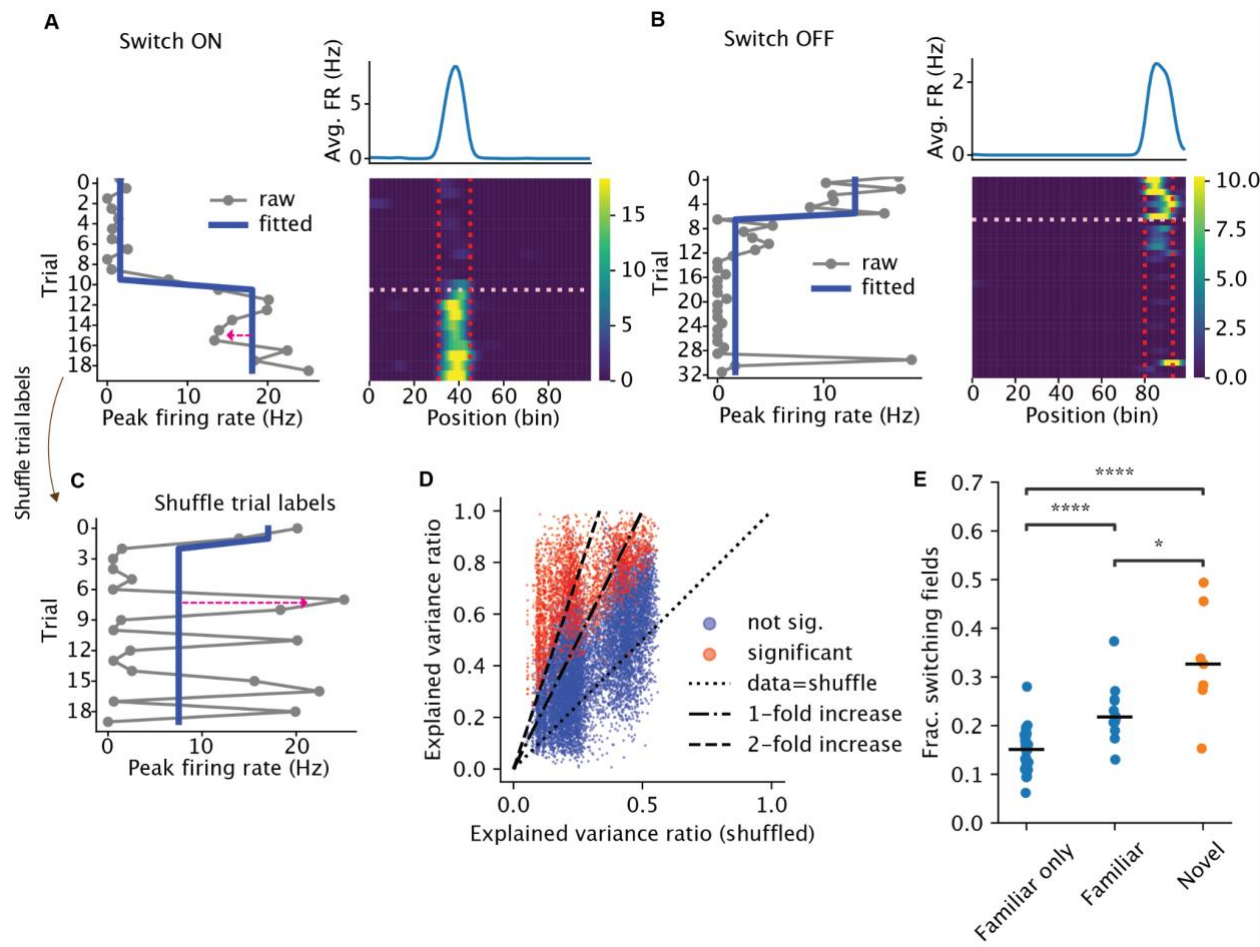
158

159 A potential artifactual source of these observations is a gradual or abrupt electrode drift in the
160 tissue, resulting in the spurious appearance/disappearance or changing firing rates of the
161 recorded neurons. Several observations and control analyses mitigate against such an
162 explanation. First, the majority of place fields were stable across the entire session and the
163 switching neurons were embedded among them (Fig. 1A). Second, comparison of the spike
164 amplitudes during pre-experience and post-experience sleep demonstrated that the firing
165 waveforms across the two sleep sessions did not vary differentially between switching and stable
166 neurons (Fig. S1A). Finally, neurons with multiple place fields simultaneously showed stable
167 and switching place fields (see examples in Fig. 5E; Fig. S1C), a strong support for the recording
168 stability despite switching fields.

169

170

171



172 **Figure 2. Place cells exhibit discrete switching of firing rate.** A- B) Examples of place cells with place
173 fields that switched ON (A) or OFF (B). Bottom right is the ratemap, i.e., firing rate (color) as a function of
174 position (X axis) and trial (Y axis). Vertical lines mark the boundary of the place fields. The horizontal line
175 marks the switch trial. Bottom left is the peak within-field firing rate across trials. The red arrow in A
176 highlights the reconstruction error. Blue line is the fitted step function. Top right is the trial-averaged
177 ratemap. C) Peak within-field firing rate from A, with the trial label shuffled. D) Explained variance ratio
178 from the best change point model, data vs shuffle. Each dot is a place field, colored by whether the field
179 had significant switching. E) Each dot is the fraction of switching fields from one session, grouped by
180 whether the session came from an animal that only experienced the familiar environment ('Familiar only',
181 n=34, median=0.15), was a familiar environment session but came from an animal that also experienced
182 the novel environment on that day ('Familiar', n=12, median=0.22), or was a novel environment ('Novel',
183 n=8, median=0.3). Horizontal bars are the medians. Two-sided Wilcoxon rank-sum test: Familiar only vs
184 Familiar, p= 4 x 10⁻⁵; Familiar vs Novel, p= 0.01; Familiar only vs Novel, p=1.7 x 10⁻⁵.

185
186
187

188 To illustrate the robustness of the change-point model, we compared it to an alternative model,
189 which poorly captures abrupt, step-like changes in firing rate, but which can accurately describe
190 the gradual emergence or disappearance of place fields. Specifically, we ran a polynomial
191 regression on each place field's firing rate with the trial number as the independent variable.
192 Importantly, we matched the number of free parameters between the change point and
193 polynomial regression models. For instance, a one-change point model has two parameters
194 specifying the means of the two segments and was compared with a linear regression model
195 (which also has two parameters: slope and intercept). An N-change point model has N+1
196 parameters and was compared with a regression model with Nth order polynomial (Fig. 3A-C).
197 The change point models explained more variance for more than 96% of the place fields across
198 all model complexities (Fig. 3D-F, left column). In contrast, polynomial regression explained
199 more variance than the change point model for the population vector decorrelation (Fig. 3D-F,
200 right column). Altogether, these analyses revealed that individual place fields tend to exhibit
201 discrete and step-like changes, in contrast to gradual and continuous changes in the population-
202 level representation.

203
204 One might object that by averaging across trial pairs with the same trial lag, our analysis on the
205 population vectors smoothed out potential "jumps" in the population vector. We therefore
206 applied the model comparison to the population vectors themselves (instead of the correlations
207 previously) (see Methods). We found the two models were largely comparable at explaining the
208 data, with more sessions (60-70%) better explained by the gradual model, and the distribution of
209 R^2 significantly biased towards continuous models (Fig. S2G). These analyses confirmed that
210 overall, the change in population was relatively gradual, but did not rule out the possibility of
211 occasional jumps that were difficult to distinguish from gradual (e.g. Fig. S2A-C).

212
213 A change point model stipulates an instantaneous "step-like" change in firing rate. Are these
214 changes really abrupt, or do they emerge over a small number of trials? Is the change a "step" or
215 a "ramp?" We reasoned that if the firing rate were slowly ramping up (resp. down), it would take
216 multiple trials to move above (resp. below) the model's predicted firing rate after a change point
217 (Fig. 3H, left). Alternatively, if the firing rate were an abrupt step, the first passage time above or
218 below the predicted firing rate would be quicker (Fig. 3H, right). Indeed, assuming that trial-to-
219 trial firing rate fluctuations following an instantaneous step up/down are symmetric around the
220 mean, the distribution of first passage times follows a negative binomial distribution (see
221 Methods). Empirically, we found that 75-77% of first passage times happened in fewer than two
222 trials and the distribution of passage times resembled the expected negative binomial distribution
223 (Fig. 3I-K). Therefore, calling the changes "discrete" or "step-like" is warranted.

224

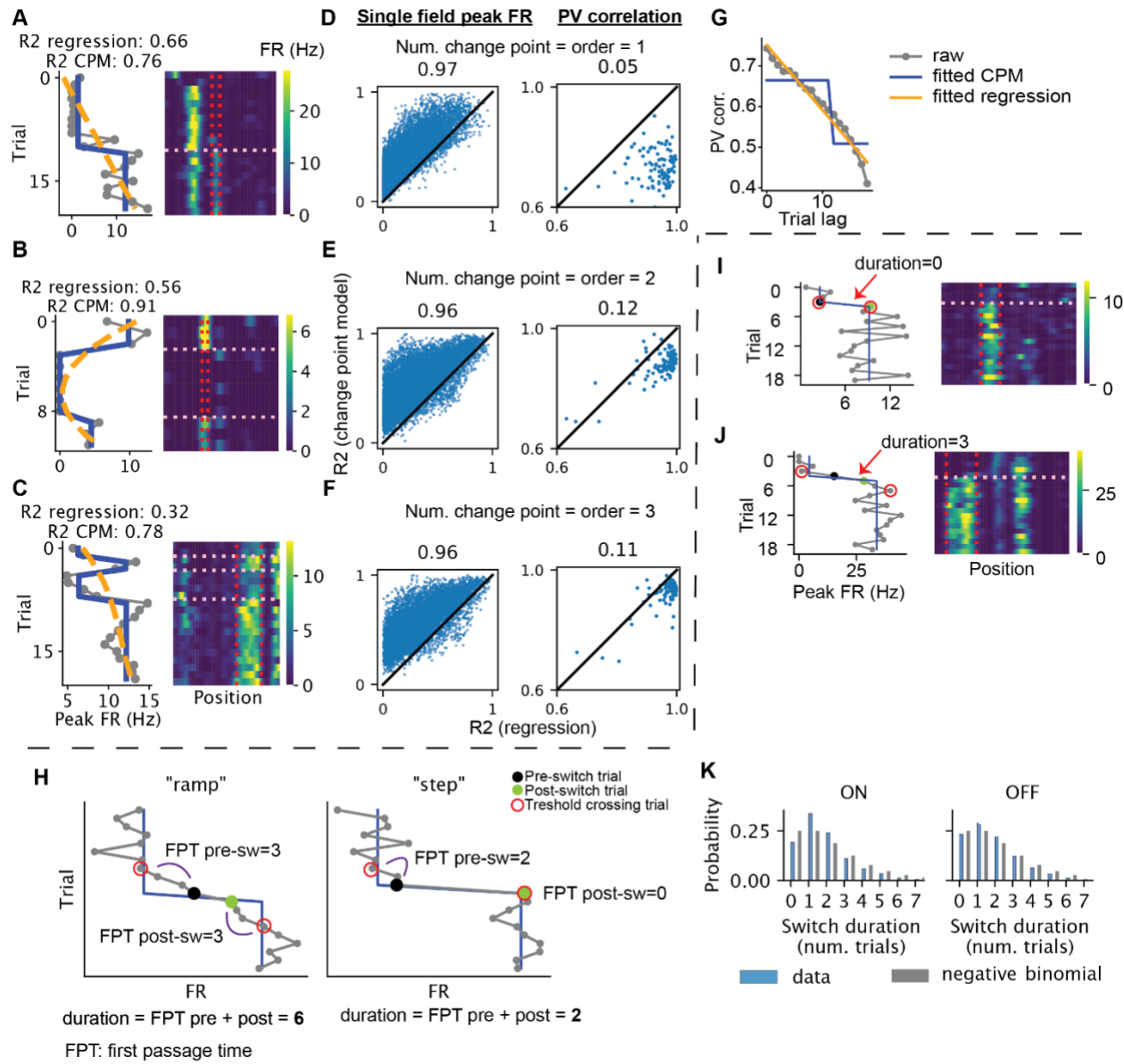


Figure 3: Discrete and continuous models of the trial-to-trial changes of within-field firing rates and population vectors. A-C) Example neurons illustrate the comparison between change point model versus a continuous polynomial regression model. Left panel, gray: within-field peak firing rate as a function of trial, blue: fitted change point model (i.e., a step function), orange: fitted polynomial regression. Right panel: ratemaps of the selected neuron. The vertical lines mark the boundary of the place field, while the horizontal line marks the detected change points. Neurons A,B and C have one, two and three change points/polynomial order, respectively. D-F) Explained variance ratio of the change point model versus that of the polynomial regression for each place field (left) and the population vector from each session (right, different turns of the T maze and different directions of the linear maze were treated separately). For individual place fields, the models are fitted to the within-field firing rate across trials. For population vectors, the models are fitted to predict population vector correlation (averaged across trial pairs) using trial lag. G) Example of the comparison between a discrete change point model and a continuous polynomial regression model (CPM) for the population vector correlation as a function of trial lag. H) Schematics demonstrating the differences in first passage time (FPT) of threshold crossing in a “ramp” (left) vs “step” model (right). Threshold crossing is defined as above the predicted firing rate by the step model post-switch-ON and below the predicted pre-switch-ON firing rate. Vice versa for OFF. Post-switch trial is the change point given by the change point detection, and pre-switch trial is one trial before. I-J) Examples demonstrating switching with different switch durations, measured by the number of trials between the first pre-switch and post-switch threshold crossing trial (red circle), minus one. K) Distributions of the switch durations for switch-ON and OFF (blue), compared with a negative binomial ($p=0.5$) with two successes (grey).

226

227 We have so far shown that a continuous drift model better characterizes the population change
228 within a session, whereas a discrete step model better describes the changes of the individual
229 place cells. We next sought to establish a relationship between the two. In other words, how
230 much does switching contribute to the drift of the population vector? To answer this question, we
231 grouped the place cell population into the “switchers” (cells with at least one switching field) and
232 “non-switchers” (cells with no switching fields). The population vector of the switching
233 population decorrelated faster than that of the non-switching population in both familiar and
234 novel environments (Fig. S3).

235

236

237 Factors that affect the rate of switching

238 Are “switches” in place field activity affected by sensory, cognitive, or behavioral factors? To
239 investigate, we used a Poisson generalized linear model to predict the number place field
240 switches per trial within five distinct segments of the maze (delay zone, central arm, left/right
241 choice arm, return side arm, and pre-delay zone; Fig. 4K). The number of switches was predicted
242 from four categorical variables—animal identifier, maze segment (“position”), current trial

243 correct/incorrect, and previous trial correct/incorrect, and three numeric variables: trial number,
244 average speed, and number of active place fields. The model explained 20% of the deviance for
245 switching ON and 14% for switching OFF. We examined the importance of each predictor by
246 leaving it out and computing the decrease in cross-validated explained deviance, compared to the
247 full model. We found that the variables that explained most of the variance were the animal
248 labels (i.e., individual differences), the maze corridors, and the number of place fields, for both
249 switching ON and OFF fields (Fig. 4A, C, F, G). Trial numbers (z-scored within a session)
250 contributed less to switching ON but more to switching OFF. The contribution from position and
251 trial suggested the occurrence of switching was not homogeneous across space and time.
252 Although the distribution of switching across arms was variable across sessions and
253 animals (Fig. S4), consistently more ON/OFF switching occurred in the delay zone (Fig. 4B, G,
254 E, J). However, we did not find any reliable behavioral signature (average speed, variability of
255 speed, fraction of time spent locomoting; see Methods) or neural signature (average pyramidal
256 cell or interneuron activities, E/I ratio) that separated the delay zone from other parts of the maze
257 (Fig. S5). As expected, switching probability decreased as a function of the trial number,
258 reflecting the graded influence of novelty discussed above¹⁵ (Fig. 4D, I). By contrast, average
259 locomotion speed did not change as a function of trials (Fig. S6C). Correct or incorrect arm
260 choice on the current or previous trial did not predict the occurrence of switching (Fig. 4C, H).
261 Leaving out locomotion speed or coefficient of variation (CV) of speed did not reduce the
262 model's ability to predict held-out data (Fig. 4A, F). Nor did we find a clear linear relationship
263 between speed and the normalized (i.e., divided by the number of fields) switching count (Fig.
264 S6A-B).
265

266

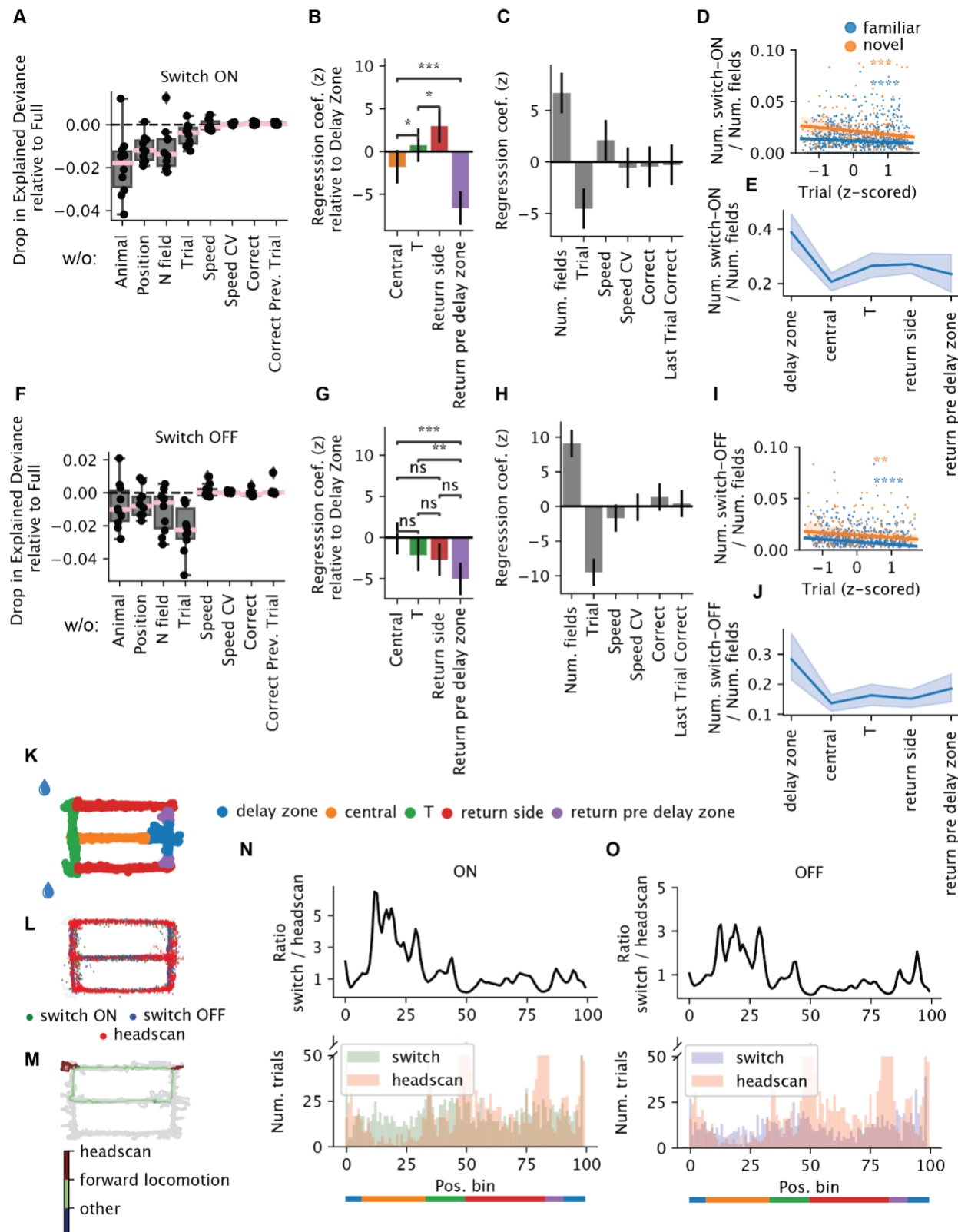


Figure 4. Spatial-temporal and behavioral modulation of switching.

A-C) Poisson generalized linear model (GLM) predicting the number of switch-ON occurrences per arm and trial within one session (n=5131). A) Drop in explained deviance relative to the full model when one predictor is removed in the GLM. Each dot is one random split in the five-fold cross-validation. B) Spatial regression coefficients, in standardized unit: each variable represents the gain in the probability of switching when the animal is in one arm relative to the delay zone. Error bars reflect 95% confidence intervals (CI). C) The rest of the regression coefficients. D) The number of switch-ON occurrences normalized by the number of fields as a function of trial (z-scored within each session for comparison across sessions with different number of trials). Blue, familiar; orange, novel (Familiar: n = 1029, Pearson $r = -0.15$, $p = 1.3 \times 10^{-6}$; Novel: n = 281; Pearson correlation $r = -0.23$, $p = 1.3 \times 10^{-4}$). E) The number of switch-ON occurrences normalized by the number of fields as a function of the arms. Each data point is one session. Shaded region reflects the 95% CI. F-J) Similar to A-E), but for switching OFF occurrences. I) (Familiar: Pearson $r = -0.2$, $p = 3.3 \times 10^{-11}$; novel: Pearson $r = -0.18$, $p = 2.7 \times 10^{-3}$). K) Schematic of the maze, with each arm colored differently. L) Detected head scanning events projected onto the maze. M) Distribution of the headscans and switches on the maze for one example session. N-O) Top: the ratio as a function of position between the number of trials when switch-ON (O) / OFF (P) occurs and the number of trials when headscans occurs. Bottom: the number of trials when switches (green or purple) / headscans (pink) occur as a function of position.

267

268 Although we failed to find behavioral correlates of place field switching, it is possible that some
269 specific behaviors could induce novel place fields or make them disappear. Indeed, it has been
270 reported that exploratory head scanning in rats was predictive of the emergence of novel place
271 fields²⁵. In our experiments, most head scans were detected in the reward area (position 50,
272 between green and red sections) while head scans in the central arm were rare (Fig. 4N, O). We
273 found no reliable relationship between field switching and incidence of head scanning (Fig. 4O,
274 P).

275

276 Field switching was not restricted to spatial tuning. The firing rates within place fields can vary
277 substantially in the central arm of the maze, depending on the animal's future choice in the
278 coming turn, known as "splitter fields" ^{26,27}. We found that the splitter feature of hippocampal
279 neurons could also switch ON and OFF at any trial of the session, similar to place fields (Fig.
280 S7). Thus, field switching is not confined to space but appears to be a generic property of
281 hippocampal neurons.

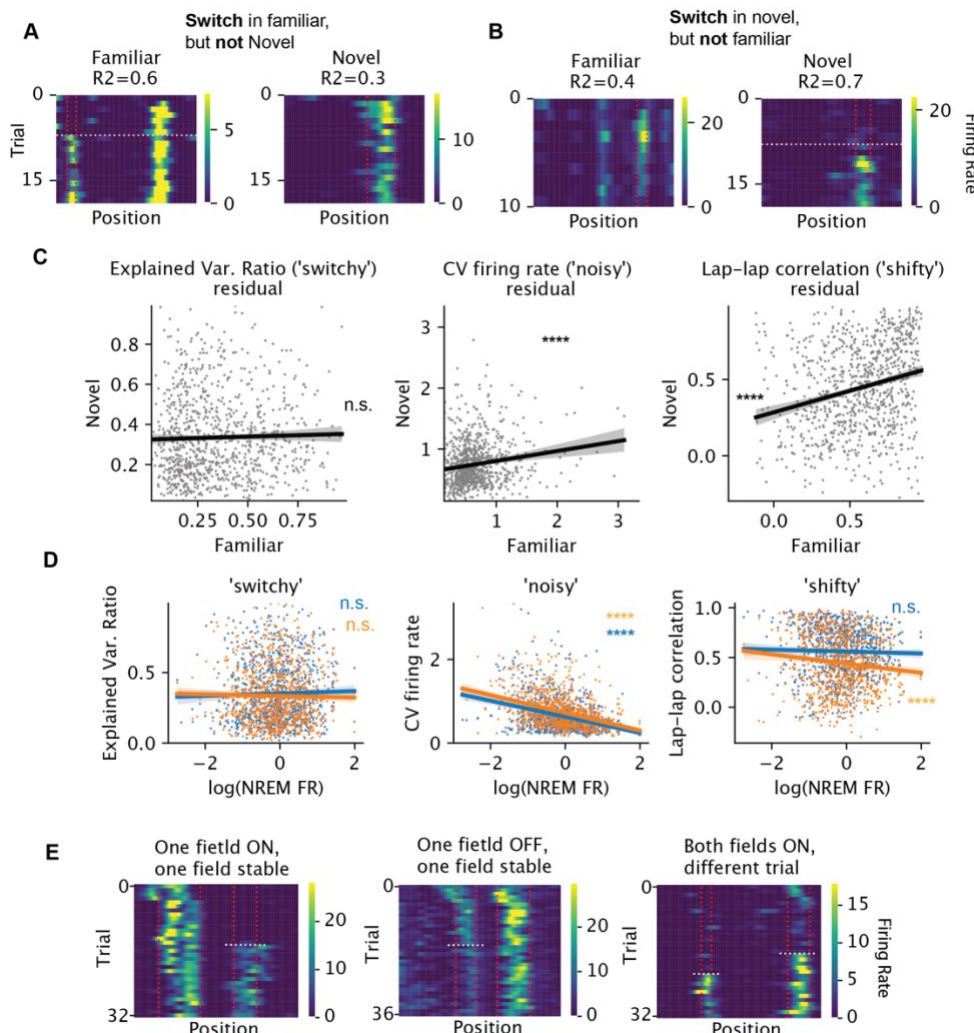
282 **Switching: neuron or circuit property?**

283 Is switching an intrinsic property of the neuron or is it controlled by the circuit in which the
284 neuron is embedded? If switching were an intrinsic property, we would expect each neuron to
285 exhibit the property consistently (i.e., switch or not switch) in different environments. We
286 observed individual neurons with a switching field in a familiar context and a stable field in a
287 novel context and vice versa, suggesting switching might not be intrinsic to the neuron (e.g., Fig.
288 5A, B). To quantify this observation, we developed a continuous metric to measure the extent to

289 which the trial-to-trial variability of the neuron is dominated by discrete switching (see
290 Methods). We found no correlation of the switchiness across the two contexts (i.e. familiar and
291 novel; Fig. 5C, left). In contrast, two other measures of variability were correlated across
292 environments (Fig. 5C, right two columns): (a) the CV of the mean within-field firing rate across
293 trials, which measures how noisy the within-field firing is and (b) the lap-to-lap correlation of the
294 firing ratemaps, which measures how jittery the spatial tuning is (examples in Fig. S8). To be
295 sure that the results are not affected by the conservation of firing rates across contexts²⁸, the
296 correlations were performed on the residual of the metrics, after the mean firing rate during non-
297 REM sleep was regressed out (Fig. 5C-D). Overall, these findings suggest that some forms of
298 firing variability, but not switchiness, are intrinsic to individual neurons.

299

300 Switching appeared to stabilize within-field firing rates for the new place fields. Specifically,
301 switch-ON fields had lower CV of firing rates within the five trials after the switch, relative to
302 trial-to-trial variability in non-switching fields over five trials taken either from the beginning or
303 middle of the session (Fig. S10A, D). Further, we observed neurons with two or more place
304 fields whose individual fields switched ON/OFF independently from one another. In some cases,
305 one field was stable while the other field switched (Fig. 5E, left and middle; quantifications in
306 Fig. S9A-D). In other cases, switching in one field occurred on different trials than switching in
307 another field (Fig. 5E, right). Out of 781 place field pairs that belonged to the same place cell
308 and both switched, only 41 (5%) switched on the same trial. Together, these results suggest that
309 switchiness is not an intrinsic property of individual neurons.

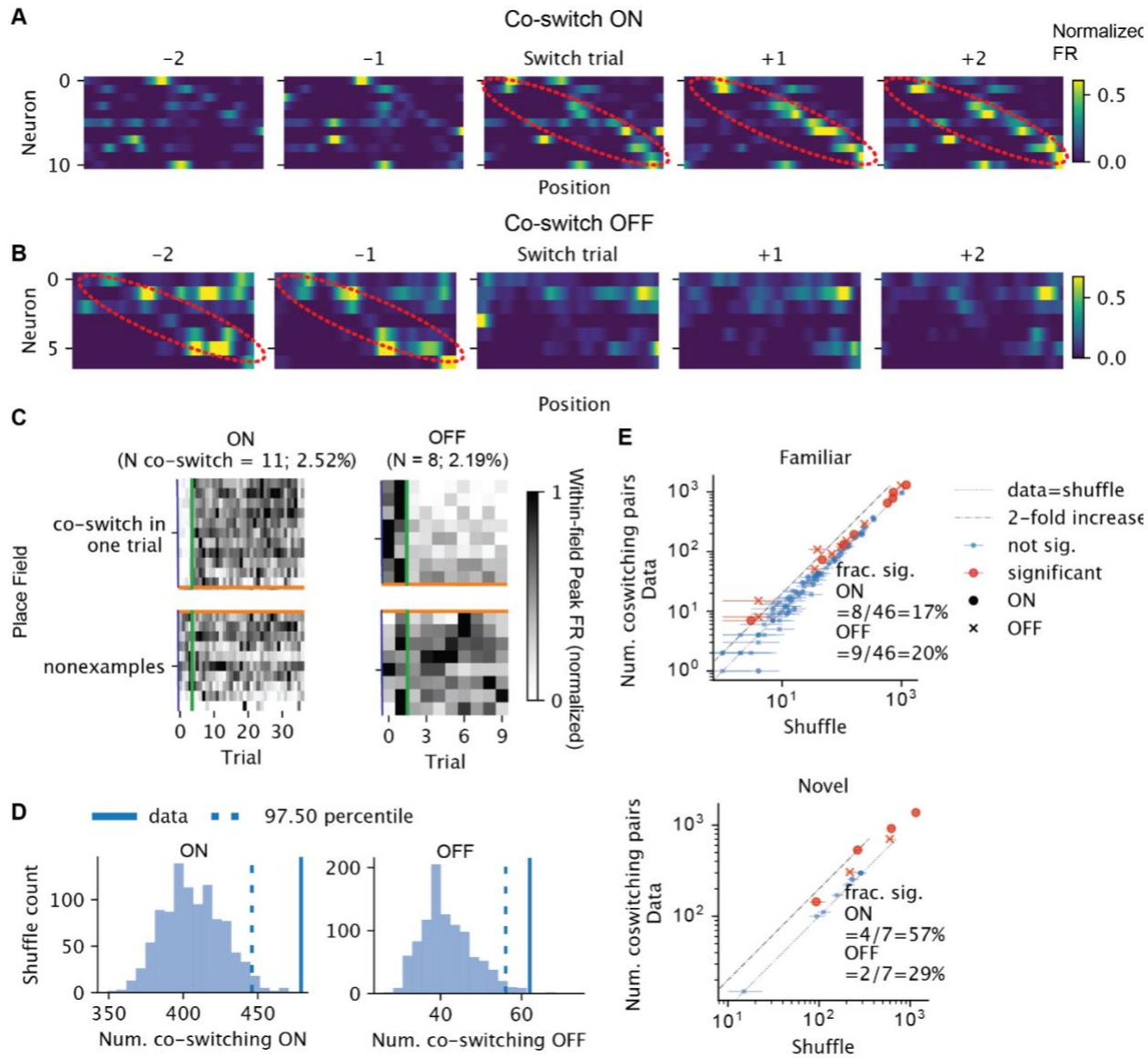


310

Figure 5. Switching is not a single-neuron property. A) Example neuron with no switch-ON field in the familiar and with switch-ON field in the novel maze. R^2 : explained variance ratio of the one-change point model. Vertical lines mark the field boundary and the horizontal line marks the switch trial. B) Example neuron with switch-ON field in the familiar but no switch-ON field in the novel maze. C) For each neuron (per dot, $n = 955$), the relationship between familiar and novel maze for each metric of variability (per column) is shown, after regressing out the effect of firing rate during NREM sleep. The firing rates were first log-transformed. The residuals are significantly correlated across environments for CV of within-field peak firing rate (left, $t = 4.8$, $R^2 = 0.02$, $p < 10^{-5}$) and lap-lap ratemap correlation (middle, $t = 7.9$, $R^2 = 0.06$; $p < 10^{-14}$), but not for the explained variance ratio from the change point model (right, $t = 0.9$, $R^2 = 0.0008$, $p = 0.37$). The errorbands show 95% CI for the regressions. D) For each neuron (per dot), the relationship between each metric of variability (per column) and its log-firing rate during NREM sleep. Blue and orange: familiar and novel environments, respectively. (Standardized linear regression coefficients and p values: noisy: familiar: $t = -11.1$, $p = 3.6 \times 10^{-27}$, novel: $t = -12.6$, $p = 1.5 \times 10^{-33}$; shifty: familiar: $t = -0.8$, $p = 0.4$, novel: $t = -3.6$, $p = 0.000326$; switchy: familiar: $t = 0.9$, $p = 0.4$; novel: $t = -0.6$, $p = 0.5$). E) Examples of subfields of a neuron showing different switching behavior.

311

312 If switching is not a cell intrinsic property, it may be driven by a circuit-level mechanism. For
313 example, BTSP-induced plateau potentials may co-occur in multiple neurons in the same trial,
314 suggesting the possibility that groups of neurons “co-switch” ON. We found that in each trial, a
315 small subset of the place fields (up to 5%) switched ON/OFF and sometimes tiled the track (see
316 example in Fig. 6A-C). We examined whether these fields switched together in the same trial
317 (which we call “co-switching”) or by chance. We created a null distribution for the number of
318 pairs of place fields that co-switched ON/OFF on at least one trial by circularly shifting the
319 switch trials for each field independently by a random amount (Fig. 6D). We then tested whether
320 the number of pairs of fields that co-switched exceeded the shuffled pairs and found that 17%
321 (20%) of the familiar sessions and 57% (29%) of the novel sessions showed at least one trial
322 with significant co-switching ON (OFF) (Fig. 6E). Together, these findings suggest that the
323 switching feature of a field reflects the flexible partnership between the neuron and different
324 assemblies, rather than intrinsic property of the neuron.



325

Figure 6: Network coordination of switching. A) Activities of example neurons whose fields co-switched ON in the vicinity of the co-switching trial. Each heatmap is the rate map for different neurons (row) for one trial. The rows are sorted by the locations of the place fields that switched together. The color reflects the normalized firing rate. The x-axis is position. The emerging sequence is highlighted in red ellipsoids. B) Similar to A, but for fields that switched OFF together. The fading sequence is highlighted in red ellipsoids. C) Within-field peak firing rates per field across trials (normalized across all trials), for the same set of neurons as in A. Each row is a field. Above the orange lines are the fields that co-switched ON at the trial marked by the green vertical lines, whereas below are the randomly selected fields that did not switch ON that trial. Left contains the fields of the neurons shown in A and right contains the fields of the neurons shown in B. D) Shuffle test result for the number of pairs of fields that co-switched ON on some trials, for the session in A (left) and B (right). E) For each session, the number of co-switching pairs vs shuffle median. The error bars mark the 95 CI from shuffle tests.

326

327

328

329

330

331

332 Red dots are sessions with significant co-switching of neurons. Circles and crosses correspond to co-
switching ON and cross OFF fields, respectively. Top, familiar and bottom, for novel context.

333

334

335 **Pre-existing dynamics constrain switching**

336 Can a spontaneously emerging place field emerge anywhere on the track? BTSP induction
337 experiments suggested that place field could form anywhere on the track, if enough current is
338 injected into the cell to form a plateau potential¹¹. Other place field induction experiments
339 stimulating a larger number of neurons simultaneously failed to induce place fields in a highly
340 localized manner^{29,30}, highlighting the network constraint on the formation and remapping of
341 place fields³¹. We therefore hypothesized that pre-existing dynamics constrain the spontaneous
342 formation and disappearance of new place fields, such that the formation should be biased by the
343 subthreshold activities before the formation, and disappearance should not eliminate the spatial
344 bias in the subthreshold activities post-disappearance.

345

346 To examine the spontaneous emergence and disappearance of place fields, we focused on the
347 subset of switching fields whose average within-field peak firing rate pre-switch-ON/post-
348 switch-OFF was below the threshold of place field detection (60% of the switching ON, 20% of
349 the switching OFF). Indeed, we found that even before the emergence of the new place field, the
350 firing rates within the future place fields were already elevated relative to the mean rate recorded
351 outside of the future place field for the majority of the neurons (Fig. S11A, C, E). Similarly, the
352 firing rates remained elevated within the previous place field after the field had switched-OFF
353 (Fig. S11B, D, F). Thus, within-session switching seems to reflect “unmasking”/“masking” of
354 preexisting/persisting place fields (Valero et al., 2022; Samsonovich and McNaughton, 1997).

355

356 A natural next question regards the timescale at which place fields preexist/persist. Spatial
357 representation drifts across days (Rubin et al., 2015) and place fields can form spontaneously via
358 BTSP (Bittner et al., 2015; Priestley et al., 2022). It is therefore plausible that place fields that
359 emerge during the experiment are “brand new” and would not have existed on the previous day,
360 reflecting drift across days. However, we found the opposite. We examined a two-photon
361 calcium imaging dataset (Hainmueller & Bartos, 2018), where mice ran on a virtual linear track
362 for multiple days. Every 5-10 trials, the mice were teleported between a familiar environment
363 and an environment that was novel on the first day of the experiment (Fig. 7A, B). In many
364 cases, we observed place fields that switched within-session made repeated appearance across
365 multiple days, suggesting a preexisting constraint on where place fields can be expressed for a

366 given place cell. For example, a place field that switched ON on day 2 could be found stably on
367 day 1 (Fig. 7C). In another example, a field switched OFF on day 1 and re-emerged on day 2.
368 Overall, we found that even on the day before the emergence the new place field, the firing rates
369 within the future place fields were already significantly elevated relative to the mean rate
370 recorded outside of the future place field (Fig. 7E,G). Similarly, the firing rates remained
371 elevated on the next day within the previous place field after the field had switched-OFF (Fig.
372 7F, H). Thus, even when the place fields are silent for an extended period (i.e., before switching
373 ON or after switching OFF), they are still subject to the constraints imposed by the network.
374

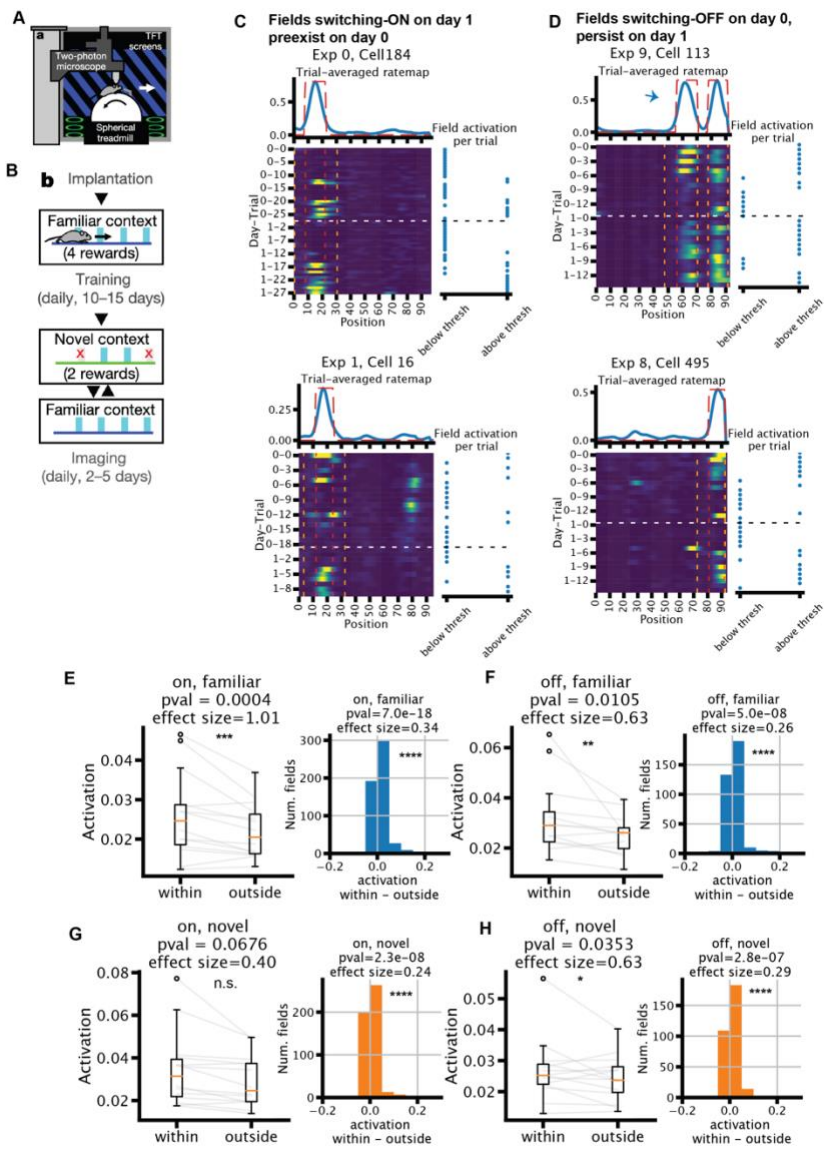


Figure 7: Switching is constrained by pre-existing fields.

A) Experimental setup of the imaging experiment. B) Behavior timeline. C-D) Example neurons that had a place field that switched ON on the second day (day 1) (C) or was OFF on the first day (day 0) (D). Top: trial-averaged ratemap in blue, with field mask in dotted red line. Bottom left: ratemap; red vertical lines mark the boundary of the fields, while orange vertical lines mark the “outside” region for the quantifications in E-H. White horizontal line marks the change in the day. Bottom right panel: binary variable of whether the within-field activation is above the place field detection threshold at each trial. Arrow in D (top) marks the place field of interest among the two fields. Note D (bottom) is an example for both scenarios in C and D. E-H) Quantifications of within- versus outside-of-fields activation (n=14). For fields that switch ON (E,G) on the second day, the quantification is done on the first day using the field detected on the second day. The opposite is true for fields that switch OFF (F, H), i.e., detected on the first day and quantified on the second day. Left: median dF/F across trials, averaged across all fields within one session, separated into within vs outside of the place fields. Right: histogram of within- minus outside of field dF/F of all fields pooled across sessions. Wilcoxon rank-sum tests and Cohen’s d are used for significance test and effect size.

376

377 **Discussion**

378 We found that hippocampal place fields can abruptly and spontaneously appear, disappear or
379 change firing rates over the course of a recording session, resulting in consistent trial-to-trial
380 turnover and gradual population-level drift in the spatial representation. These “switches” in
381 individual place fields occurred in any part of the maze without apparent behavioral correlates.
382 Switching was not exclusive to place fields as choice-predicting (“splitter”) fields also showed
383 regular turnover. The rate of drift was accelerated by novelty. Switching was not an intrinsic
384 property carried by single neurons: different place fields belonging to the same neuron could
385 have independent switching properties. But pairs of place fields from different neurons switched
386 on the same trial more often than chance, reflecting population-level coordination. Finally, when
387 place fields formed spontaneously, the locations were constrained by the pre-existing spatial bias
388 in the subthreshold activities before the formation. The constraint also persisted after the
389 disappearance. These constraints extended beyond single sessions into multiple days.
390

391 **Robustness of the change point model**

392 Representational drift is often studied in a trial-averaged manner and described as “gradual” in
393 both population activity and single neurons^{3,4,6,32–36}, but see Marks & Goad⁷. However, these
394 reports relied on qualitative reports of aggregated statistics and did not explicitly model the drift
395 dynamics of single neurons. We leveraged change point detection, shuffle tests, and comparison
396 to polynomial regression to rigorously arbitrate the issue of gradual vs sudden change.
397 Decorrelations of PV averaged across trial pairs were gradual, while changes in the peak within-
398 field firing rate were sudden, highlighting the necessity of careful model comparison with single-

399 cell and single-trial resolution. Our modeling framework also allowed us to detect changes in
400 within-field firing rates beyond simple emergence of place fields, which was the focus of studies
401 of BTSP^{11,12,15}. By expanding our analysis to a broader variety of firing rate changes, we gained
402 a more complete picture of the persistent and sudden changes of place field features. They also
403 gave us the power to determine the contribution of the “switchers” to the population level drift
404 and to examine the coordination of switching in the population.

405 **Interpretations of representational drift**

406 The term “representational drift” refers to the changing relationship between external variables
407 (image, odor, space etc.) and neuronal activity. One interpretation hypothesized the homeostatic
408 re-adjustment of synapses and firing rates^{37,38} as a driver for drift. An implication is that the
409 longer the elapsed time between retesting, the larger the drift. In support of this hypothesis,
410 longer testing intervals lead to larger decorrelation^{4,36}. However, recent experiments showed a
411 greater role of the amount of awake experience in the degree of drift than time *per se*^{33,34}. The
412 within-session drift we observed is consistent with these observations.
413

414 Another potential driver for drift could be changing attentional and behavioral states. The
415 implicit assumption of drift is that spiking patterns correspond to or “represent” some external
416 physical features^{1,39}. Thus, the spiking patterns can change when the animals attend to different
417 external features⁴⁰⁻⁴². Consequently, drift could be induced by changes in animal’s behavior or
418 attentional states⁴³⁻⁴⁶. In particular, Monaco et al.²⁵ reported that exploratory head movement can
419 reliably induce novel place fields in rats. We found though that such “stereotypical” behavior
420 was not necessary to induce firing rate changes in mice. In addition, switching could occur
421 everywhere and all the time, suggesting that it is not induced by particular events.
422

423 Here we offer an alternative explanation for the drift, that the neuronal circuits are perpetually
424 reorganized through their internal dynamics^{47,48}. We propose that particular changes in
425 attentional behavior or physiological states (like sleep) are not necessary for reorganization,
426 although they can modulate the rate of reorganization. Fluctuations in the nervous system may
427 trigger spontaneous plateau potentials that induce BTSP and change the tuning¹¹, corresponding
428 to the switch-ONs. Alternatively, Kispeksky et al.⁴⁹ showed in a biophysical model that small
429 changes in AMPA conductance could lead to an abrupt increase in firing rate due to the dynamic
430 properties of the ionic currents. Switch-OFFs (which were not explicitly described via BTSP)
431 might be triggered by the switch-ONs in other pyramidal cells via interneurons to maintain E-I
432 balance^{50,51}. In support of this interpretation, optogenetic stimulation of hippocampal pyramidal
433 cells led to the appearance and disappearance of place fields (“remapping”) both inside and
434 outside the stimulated part of the maze, via affecting monosynaptic drive of interneurons^{29,31,52}.
435 Similarly, long-term potentiation of the CA3-CA1 connections both induced and abolished place
436 fields transiently but reverted to their default fields with extended time⁵⁰.
437

438 Our postulation that perpetual changes of neuronal dynamics are internally organized does not
439 diminish the role of behavioral effects and external inputs. Indeed, we showed that place fields in
440 the delay zone had a higher rate of switching ON/OFF, and place fields tended to switch more
441 frequently in earlier trials, which could be due to different behavioral, attentional, and
442 motivational states at particular places and times. Head scanning, active exploration, and

443 attention to novel and salient cues may effectively trigger instantaneous or slow modification of
444 firing patterns and/or affect the temporal rate of population vector decorrelations. Thus, STDP-
445 induced slow and BTSP-induced quantal plasticity mechanisms likely co-exist and combine the
446 advantages offered by each mechanism.

447 **Properties of the preexisting constraint**

448 The presence of subthreshold place fields in “silent” neurons has been shown by unmasking their
449 spiking fields by sustained or transient depolarization^{53,54}. These subthreshold fields are
450 hypothesized to reflect preexisting constraints imposed by hippocampal cell assemblies.
451 Consistent with this hypothesis, we observed persistent place fields that spontaneously formed
452 and disappeared across multiple days. Given that switching comprises preexisting/persistent
453 place fields, it is possible that fluctuations of excitation and inhibition could unmask the place
454 field even without the need for BTSP or other forms of drastic plasticity^{49,53,54} by moving
455 population activity from one attractor to the next.
456

457 Given the constraint on place field locations that we observed across two days, how could large
458 changes in population-level representation happen across many weeks⁴? We hypothesize that the
459 pre-existing constraint merely biases the expression of place fields, but does not fully determine
460 it. On a timescale of two days, place fields exhibit mostly ON and OFF switching in a fixed
461 range of locations. On a slower time scale, however, the tendency of ON and OFF switching
462 could change. For instance, a neuron might switch ON less frequently and eventually develop a
463 new place field in a different location. The constraint itself is a reflection of the population
464 activity and connectivity, and therefore could also slowly change as the population drifts, making
465 it easier for cells to develop place fields in new locations. Our findings and explanation are
466 consistent with work from Geva et al.³³, which finds that place field location shifts over days are
467 not random but become progressively larger over longer time intervals. We find that this
468 constraint is present even for unstable fields that emerge and disappear on the timescale of trials.
469
470
471
472
473
474
475
476

477 **STAR+METHODS**

478 Detailed methods are provided in the online version of this paper and include the following:

479 **KEY RESOURCES TABLE**

480 **RESOURCE AVAILABILITY**

481 **Lead contact**

482 Further information and requests should be directed to the lead contact, György Buzsáki
483 (gyorgy.buzsaki@nyulangone.org).

484 **Materials availability**

485 This study did not generate new unique reagents.

486 **Data and code availability**

487 The electrophysiological dataset analyzed for the present study has been made publicly
488 available in the Buzsáki lab repository (<https://buzsakilab.nyumc.org/datasets>). The calcium
489 imaging dataset that support the findings of this study are available from Marlene Bartos
490 (bartos@physiologie.uni-freiburg.de) upon reasonable request. The custom analysis code is
491 available upon request.

492

493 **EXPERIMENTAL MODEL AND SUBJECT DETAILS**

494 We refer to Huszár et al.²⁰ and Hainmueller & Bartos²¹ for details on the mice used for the
495 electrophysiological dataset and the two-photon calcium imaging dataset, respectively.

496

497 **METHOD DETAILS**

498 **Datasets**

499 For details on animal surgery, training, recording, data preprocessing, spike sorting and state
500 scoring, we refer to Huszár et al.²⁰ and Hainmueller & Bartos²¹ for the electrophysiological
501 dataset and the two-photon calcium imaging dataset, respectively. In brief, for the
502 electrophysiological dataset, we used the chronic silicon probe recordings from hippocampal
503 CA1 region in n=11 mice. The animals were trained on a spatial alternation task on a figure-eight
504 maze. Animals were water restricted before the start of experiments and familiarized to a
505 customized 79 × 79 cm² figure-eight maze raised 61 cm above the ground. Over several days after
506 the start of water deprivation, animals were shaped to visit alternate arms between trials to
507 receive a water reward. A 5-s delay in the start area (delay area) was introduced between trials.
508 The position of head-mounted red LEDs (light-emitting diodes) was tracked with an overhead
509 camera at a frame rate of 30 Hz. Animals were required to run at least ten trials along each arm
510 (at least twenty trials total) within each session. In all sessions that included maze behavior,
511 animals spent ~120 min in the homecage before running on the maze and another ~120 min in
512 the homecage afterward for sleep recordings. All behavioral sessions were performed in the
513 mornings (start of the dark cycle). A subset of n=3 mice were exposed to novel environments in
514 addition to the familiar figure-eight maze. After the shaping phase described above, animals
515 underwent recording sessions consisting of a ~120-min homecage period, running on the figure-
516 eight maze, ~60-min homecage period, running in a never-before experienced environment,
517 followed by a final ~120-min homecage period. The novel environments included two distinct
518 linear mazes and a different figure-eight maze. Mazes were placed in distinct recording rooms, or
519 in different corners of the same recording room, with distinct enclosures to ensure unique visual
520 cues. We required that the familiar sessions had no fewer than 20 trials in total and 7 trials per
521 turn, and no fewer than 50 putative pyramidal cells. Overall, we included 46 familiar sessions
522 and 8 novel sessions. For the co-switching analysis, we further excluded a novel session because
523 it had too few trials.

524 For the calcium imaging dataset, mice were injected with AAV1.Syn.GCaMP6f.WPRE.SV4 to
525 express the calcium indicator GCaMP6f pan-neuronally in the dorsal CA1. The mice were then
526 implanted with a 3 mm diameter transcranial window over the external capsule after aspiration
527 of the overlying cortex and imaged with a resonant-scanning two-photon microscope (for details
528 see Hainmueller and Bartos²¹). For imaging experiments, the mice were head-fixed and ran in a
529 virtual environment resembling a linear track. The track consisted of textured walls, floors and
530 other 3D rendered objects at the tracks sides as visual cues. Potential reward locations were
531 marked with visual and acoustic cues, and 4 μ l of soy milk was gradually dispensed through a
532 spout in front of the mouse as long as the mouse waited in a rewarded location. The forward gain
533 was adjusted so that 4 m of distance travelled along the circumference of the ball equaled one
534 full traversal along the linear track. When the mouse had reached the end of the track, screens
535 were blanked for 5–10 s and the mouse was ‘teleported’ back to the start of the linear track. The
536 virtual environment was displayed on four TFT monitors (19" screen diagonal, Dell) arranged in
537 a hexagonal arc around the mouse and placed ~25 cm away from the head, thereby covering
538 ~260° of the horizontal and ~60° of the vertical visual field of the mouse. Mice were first trained
539 in the familiar virtual environment for 4–5 days. After the window implantation surgery, mice
540 were re-habituated in the familiar virtual environment until consistent reward licking. From the
541 first day of the imaging session, mice were introduced to a novel context, which had different
542 visual cues, floor and wall textures but had the same dimensions as the familiar context including
543 the four marked reward locations. On the novel track, two of these reward sites were disabled
544 (that is, the auditory cue was still given, but no reward was dispensed). Mice alternately ran on
545 the two tracks for a total of 15–30 runs on each track and day. The mice made 1–5 runs on one
546 track and then an equal number of runs on the other. The length of these trial blocks was
547 randomly varied. Imaging was performed in the same set of contexts for two to five consecutive
548 days. We only considered the CA1 recording for two days, 14 experiments in 11 animals, with
549 9828 pyramidal cells (150–1765 per session).

550 Significant calcium transients were identified, which mainly reflect burst firing of principal cells.
551 In brief, calcium traces were corrected for slow changes in fluorescence by subtracting the eighth
552 percentile value of the fluorescence-value distribution in a window of ~8 s around each time
553 point from the raw fluorescence trace. We obtained an initial estimate on baseline fluorescence
554 and standard deviation (s.d.) by calculating the mean of all points of the fluorescence signal that
555 did not exceed 3 s.d. of the total signal and would therefore be likely to be part of a significant
556 transient. We divided the raw fluorescence trace by this value to obtain a $\Delta F/F$ trace. We used
557 this trace to determine the parameters for transient detection that yielded a false positive rate
558 (defined as the ratio of negative to positive oriented transients) <5% and extracted all significant
559 transients from the raw $\Delta F/F$ trace. Definitive values for baseline fluorescence and baseline s.d.
560 were then calculated from all points of this trace that did not contain significant transients. For
561 further analysis, all values of this $\Delta F/F$ trace that did not contain significant calcium transients
562 were masked and set to zero.

563 **Behavior segmentation**

564 From the 2D position tracking, we computed the velocity in x and y directions within each time
565 bin and smoothed it with a gaussian filter (std = 10 bins), and then computed the speed using $v =$
566 $\sqrt{v_x^2 + v_y^2}$. We categorized the animal's behavior on the maze into forward locomotion,
567 immobility, and headscan. We first defined immobility as times when the speed was $< 1\text{cm/s}$. We
568 then detected headscan using a simplified version of the method used in Monaco et al²⁵.
569 Headscan events were detected by first finding times when the distance between the animal's
570 head position (reflected by the LED tracking) and the track was above a threshold of 3 cm. We
571 then extended the time both forward and backward till when the head position was "on-track",
572 distance $< 1\text{ cm}$. Both thresholds were manually adjusted to minimize type I and type II error.
573 Among these putative events, those that were shorter than 0.4s in time, and those whose start and
574 end locations had a distance greater than 20 bins were excluded. The rest of the events were
575 merged if the end of one and the start of the next were within 0.4s in time. We computed the
576 distance to the maze from one point by first sampling positions that were on the maze, and then
577 calculated the smallest Euclidean distance from that point to the position samples. We sampled
578 positions on the maze by: 1) selecting the time points where the speed was $> 10\text{cm/s}$; 2) using
579 these points to construct a map from the linearized coordinates back to the 2D coordinates using
580 linear interpolation; 3) evenly sampling 200 linearized coordinates; and 4) mapping them back to
581 the 2D coordinates. Excluding the times of immobility and headscan, as well as occasional
582 backtracking, the rest was considered forward locomotion.

583 **Ratemap calculation**

584 Only time points when animals were moving forward were included. Spikes were binned by bins
585 of 2.2cm. The spike counts and occupancies within each bin were smoothed by a gaussian filter
586 with standard deviation of 2.5. We obtained ratemaps per trial by dividing the smoothed spike
587 counts by smoothed occupancies. We then averaged over trials to obtain a trial-averaged
588 ratemap. For the imaging dataset, we first mask the dF/F traces and performed the same
589 operations on the masked traces in place of spikes.

590 **Place field detection**

591 For the electrophysiological dataset, we circularly shuffled animal's positions in time and
592 constructed trial-averaged ratemaps 1000 times to obtain a null distribution of the average
593 ratemaps per neuron. Place fields were defined as contiguous chunks of positions where: 1) the
594 empirical average ratemaps were above the 95th percentile of the null distribution; 2) the size
595 was between 4 and 30 bins; and 3) the peak firing rate within the field was above 1Hz. For the
596 imaging dataset, we circularly shuffled the animal's position labels in the ratemaps per trial and
597 then averaged to obtain a null distribution of the average ratemaps per neuron. Place fields were
598 defined as contiguous chunks of positions where: 1) the empirical average ratemaps were above
599 a threshold. The threshold for each neuron was computed as: 0.25 times the difference between

600 the peak of the average ratemap and the baseline. The baseline was defined as the 25th percentile
601 of the activity rate among all the positions and trials. The baseline was either defined using the
602 current session or all days, giving rise to a threshold and a “pooled” threshold. The final
603 threshold was the maximum between the threshold and 0.6 * pooled threshold. Including a
604 pooled threshold ensured that small fluctuations on one day would not be classified as place field
605 activity if the neuron had high activity on the other day. 2) The in-field gain, measured by the
606 average within-field activity/average outside activity had to be >3 . 3) The peak within-field
607 activity rate had to be higher than the 80th percentile of the null distribution. After detecting the
608 place fields, we computed the peak within-field firing rate per trial and the peak locations per
609 trial. For the analysis of preexisting fields, we obtained the outside region for each place field by
610 extending the field in both directions, each for 10% of the track length, until it hit the boundary
611 of the maze or another field.

612

613 For the figure 8-maze data, we separated place fields into fields that were common for both turns
614 (on the central arm) and fields that were specific for one type of turn (on non-central arms or
615 splitter cells on the central arm). The field was determined to be common to both turns if the
616 peaks detected from both turns were less than 5 bins apart and lied on the central arm, and that
617 the peak firing rates per trial were not significantly different between two turns (using
618 independent t-test). If they were, then the field was deemed a splitter field. Analysis on the place
619 field parameters (firing rate, location) were performed using all trials for the turn-common fields,
620 and only trials for one turn for the turn-specific fields.

621 **Detection of discrete switching**

622 We used a change point detection algorithm called optimal partitioning²⁴. Given the number of
623 change points (K), it searches for K changes points ($\{\tau_1, \dots, \tau_K: 1 < \tau_1 < \dots < \tau_K < \tau_{K+1} = T\}$)
624 that partitions the time series $x_{1:T}$ into $K + 1$ segments, where T is the length of the signal. Each
625 segment is associated with a cost. In our case the cost was the sum of squared error of fitting a
626 constant function within a segment: $C_1(u, v) = \sum_{i=u}^v (x_i - \underline{x}_{u:v})^2$, where $\underline{x}_{u:v}$ is the average of x
627 within u and v . The objective is to find change points that minimize the total cost: $C_{K+1}(1, T) =$
628 $\sum_{i=1}^{K+1} C_1(x_{(\tau_i+1):\tau_{i+1}})$, where the left hand side denotes the minimal cost from 1 till T given K
629 change points ($K + 1$ segments). At its core, the search utilizes a recursive relation that relates
630 the optimal value of the cost function within a segment given m change points to the optimal
631 cost within a subsection from the start of the segment to the last change point (given $m - 1$
632 change points): $C_{m+1}(u, v) = C_m(u, t) + C_1(t + 1, v)$. Starting from $C_1(u, v)$ for all pairs of
633 u, v , it recursively computes $C_m(u, v)$ for $K + 1 \geq m \geq 2$. Finally, it backtracks to find the set
634 of change points: starting from $\tau_{K+1} = T$, given $\tau_{m+1}, \tau_m = \arg \arg C_{m-1}(1, \tau_m) +$
635 $C_1(\tau_m, \tau_{m+1})$. The time complexity is $O(KT^2)$, compared to $O(T^K)$ in the naïve way. For a more
636 detailed description we refer to Truong et al.⁵⁵ for a review. We used the Python package

637 ruptures⁵⁵ to perform change point detection on the time series of within-field peak firing rate
638 over trials. We set the parameter of the minimal segment length to be two.

639
640 To determine the significance of the change points and further determine the number of change
641 points that suited the data the best, we noticed that if a step-function like structure existed in the
642 data, shuffling the data would break the structure and incur a higher cost from the change point
643 model than in the original data. This observation allowed us to determine whether there was any
644 significant discrete jump in the data. We could further determine the optimal number of change
645 points by selecting the number that led to the highest increase in cost in shuffle compared to data.
646 This way, overfitting with many change points was avoided, because increasing the number of
647 change points would also decrease the cost in the shuffle, counterbalancing the decrease in the
648 cost of the data. In practice, for each place field, we shuffled the within-field peak firing rate
649 over trials 1000 times and fit each shuffle with change point models from one change point up to
650 $\min(5, \lfloor \text{num. trials} / 4 \rfloor)$ and obtained the costs. The empirical costs were compared against the
651 shuffle to compute the P-values. We then performed a Bonferroni corrected test (with a P-value
652 threshold of 5%) to determine whether a field had any significant change points. Next, the
653 optimal number of change points to each field that had significant change points was determined
654 to be the one whose empirical cost had the lowest percentile in shuffle. Finally, we filtered
655 change points whose step sizes were < 40% of the max firing rate across trials to include only
656 relatively large changes. Although the shuffle test already tended to favor large and sustained
657 changes, the final filter filtered out only a small fraction of events.

658

659 **Metrics of variability**

660 We used two traditional metrics of variability: CV of the firing rate (“noisy”) and the lap-to-lap
661 ratemap correlations (“shifty”), plus one new metric based on the change point detection
662 (“switchy”), to measure the variability of the space-related activities of the place cells. The
663 “noisiness” measured the total amount of fluctuations of the within-field peak firing rate and was
664 computed as the standard deviation divided by the mean of the within-field peak firing rate
665 across trials. We then averaged them across fields to get one measure for one neuron. The
666 shiftiness was the Pearson correlation between the ratemaps from a pair of trials, averaged over
667 all pairs of trials, and primarily measured the shift in the location or distribution of the ratemap.
668 Neither of these metrics captured the degree of step-function like switching, which we called
669 switchiness and defined to be the fraction of variance of the within-field peak firing rate
670 explained by the change point model with one change point. (Fixing one change point is to make
671 place fields that have different optimal numbers of change points comparable). We then average
672 the switchiness per field to assign a score to each neuron.

673

674 **Continuous model of trial-dependent change**

675 We compared the discrete switching model with a continuous model for explaining both the
676 change in single place field’s activity over trials and also the decay in the population vector

677 correlations as a function of trial lags. The continuous model was a polynomial regression
678 $y(t) \sim b_0 + b_1 t + b_2 t^2 + \dots + b_k t^k$, where $y(t)$ was either the peak within-field firing rate of one
679 place field in trial t or the population vector correlation averaged over all trials pairs t trials
680 apart, b_i s were the coefficients and k was the order of the model. The fitting was done using the
681 Python library statsmodels⁵⁶.

682

683 **Model comparison applied to the population vectors**

684 To further determine whether the population vectors evolve gradually or abruptly while ruling
685 out the effect of trial averaging, we apply the change point or regression models to the
686 population vectors themselves (instead of the correlations previously). To simultaneously speed
687 up the computation and reduce the noise, we first reduced the dimensionality of the matrix of
688 population vectors (n_trial-by-(n_neuron x n_position)) to n_trial-by-n_feature, where n_feature
689 is chosen to preserve just above 95% of the variance, usually n_trial-2. Now the fitted piece-wise
690 constant function from the change point model are vector-valued functions, with change points
691 shared across the feature dimensions. The cost for one section is now the sum of the cost over all
692 dimensions. The polynomial regression models are fitted to each feature dimension
693 independently. This choice is justified since gradual changes of each dimension would add up to
694 a gradual change of the population, whereas if sudden changes occur at different times across
695 each dimension, we would not necessarily regard the population as having jumps. The explained
696 variance ratio can be obtained as usual.

697

698 **Switch duration quantification and comparison**

699 If the trial-to-trial firing rate fluctuations before and after an instantaneous step up/down are
700 symmetric around the mean, the distribution of first passage times (FPTs) follows a negative
701 binomial distribution. The negative binomial distribution models the number of tails in a
702 sequence of coin tosses before k heads occur. In our case, the coin was fair ($p = 0.5$). We defined
703 thresholds as the firing rates (FRs) predicted by the change point model. For switch-ONs, the
704 first threshold crossing post-switch was defined as the first trial when the actual FR went above
705 the predicted FR after the switch. The first threshold crossing pre-switch was the first trial
706 (counting backwards from the switch) when the actual FR was below the predicted FR before the
707 switch. Vice versa for switch-OFFs. The FPTs were defined as the number of trials between the
708 post/pre-switch trial and the first threshold crossing. The post-switch trial was the change point
709 given by the change point detection, while the pre-switch trial was the trial before the post-
710 switch trial. For each switching, we summed the FPTs pre- and post-switch to get the switch
711 duration. Since each of the FPT was expected to follow a negative binomial distribution with
712 $k = 1$, the switch duration was compared with a negative binomial distribution with $k = 2$, i.e.
713 the sum of two independent negative binomial variables with $k = 1$.

714

715 **Contribution of switching neurons to drift**

716 We grouped the place cell population into the “switchers” (cells with at least one switching field)
717 and “non-switchers” (cells with no switching fields). To ensure the sizes of the groups were
718 comparable, we sampled non-switchers to match the size of the switchers for each session ten
719 times and averaged the analysis results for Fig. 4A and B. For each subpopulation, we computed
720 the population vector correlation and took the median across all trial pairs given a trial lag for
721 each session. We next measured the magnitude of decorrelation per session by fitting a linear
722 regression on the population vector correlation, using trial lag as the regressor.
723

724 **Generalized linear model of switching**

725 We used a generalized linear model (GLM) to predict the number of switching ON/OFF per trial
726 and arm (familiar maze only). The relevant variables were aggregated per trial and arm for each
727 session and concatenated across sessions and animals. The full model was

728 $\log(y) \sim C(Animal) + C(Position) + N_field + Trial + Speed + CV_speed +$
729 $C(Correct) + C(Prev_correct)$, where y was the number of switching $C(\cdot)$ indicates
730 categorical variables. “Position” refers to the arm of the maze. “ N_field ” refers to the number of
731 fields whose peak lied in that arm. “Trial” and “Speed” were z-scored within session to aid
732 comparison across sessions and animals. “Speed” refers to the average speed within the arm at
733 the trial. “ CV_speed ” refers to the coefficient of variation of the speed within the arm at the trial.
734 “Correct” refers to whether the animal made the correct turn on the current trial, and
735 “ $Prev_correct$ ” whether the previous trial was correct. We used a Poisson likelihood function.
736 The variable selection was performed by repeating a 5-fold stratified cross-validation 10 times
737 (grouped by animal to make sure the relative sample size for different animals were maintained).
738 The fitting and cross-validations were done via the Python library sklearn.
739

740 **Quantification of pre-existing constraint**

741 To quantify the extent to which the place field preexisted (before switch-ONs) or persisted (after
742 switch-OFFs), we computed the difference between the mean within-field firing rate (or dF/F for
743 imaging) and the mean outside-of-field firing rate (or dF/F). The “outside” was defined by
744 extending the field boundary in both directions by 10% of the track length, until it hit the end of
745 track or the onset of another place field. This way we ensured that the quantification was not
746 obfuscated by the existence of multiple fields. We then took the median across trials for each
747 neuron and plotted the distribution in Fig. 7E-H (left panels). To make sure the result is robust
748 across sessions, we also averaged the within and outside dF/F across all fields within a session
749 (Fig. 7E-H, right panels).
750

751 **QUANTIFICATION AND STATISTICAL ANALYSIS**

752 All statistical details, including the specific statistical tests, are specified in the corresponding
753 figure legends. In general, for one sample and paired two samples we performed two-sided
754 Wilcoxon signed rank tests. For unpaired two samples we performed two-sided Wilcoxon rank
755 sums test. We used the Pearson correlation coefficient to measure linear correlation. Effect sizes
756 were reported using Cohen’s d. All statistical analyses were conducted using Python.

757

758 **SUPPLEMENTAL INFORMATION**

759

760 **ACKNOWLEDGMENTS**

761 We thank Isabel Low for comments on the manuscript. We thank Caleb Kemere and members
762 of the Williams and Buzsaki laboratories for feedback and support. Supported by NIH
763 MH122391, and U19 NS107616.

764 **Contributions**

765 Z.Z. and G.B. designed the research.

766

767 Z.Z., R.H., T.H. and M.B. performed the research.

768

769 Z.Z. analyzed the data.

770

771 G.B. and A.W. provided technical support.

772

773 Z.Z., A.W. and G.B. wrote the paper.

774

775

776

777 **DECLARATION OF INTERESTS**

778 G.B. is a member of Neuron's advisory board.

779

780

781

782

783

784

785

786

787

788

789

790

791

792

793 **Reference**

- 794 1. O'Keefe, J., and Nadel, L. (1978). The Hippocampus as a Cognitive Map (Oxford:
795 Clarendon Press).

796 2. Thompson, L.T., and Best, P.J. (1990). Long-term stability of the place-field activity of single
797 units recorded from the dorsal hippocampus of freely behaving rats. *Brain Res.* 509, 299–
798 308. 10.1016/0006-8993(90)90555-p.

799 3. Manns, J.R., Howard, M.W., and Eichenbaum, H. (2007). Gradual Changes in Hippocampal
800 Activity Support Remembering the Order of Events. *Neuron* 56, 530–540.
801 10.1016/j.neuron.2007.08.017.

802 4. Ziv, Y., Burns, L.D., Cocker, E.D., Hamel, E.O., Ghosh, K.K., Kitch, L.J., Gamal, A.E., and
803 Schnitzer, M.J. (2013). Long-term dynamics of CA1 hippocampal place codes. *Nat.*
804 *Neurosci.* 16, 264–266. 10.1038/nn.3329.

805 5. Sheintuch, L., Geva, N., Baumer, H., Rechavi, Y., Rubin, A., and Ziv, Y. (2020). Multiple
806 Maps of the Same Spatial Context Can Stably Coexist in the Mouse Hippocampus. *Curr.*
807 *Biol.* 30, 1467-1476.e6. 10.1016/j.cub.2020.02.018.

808 6. Schoonover, C.E., Ohashi, S.N., Axel, R., and Fink, A.J.P. (2021). Representational drift in
809 primary olfactory cortex. *Nature* 594, 541–546. 10.1038/s41586-021-03628-7.

810 7. Marks, T.D., and Goard, M.J. (2021). Stimulus-dependent representational drift in primary
811 visual cortex. *Nat. Commun.* 12, 5169. 10.1038/s41467-021-25436-3.

812 8. Jensen, K.T., Kadmon Harpaz, N., Dhawale, A.K., Wolff, S.B.E., and Ölveczky, B.P. (2022).
813 Long-term stability of single neuron activity in the motor system. *Nat. Neurosci.* 25, 1664–
814 1674. 10.1038/s41593-022-01194-3.

815 9. Markram, H., Lübke, J., Frotscher, M., and Sakmann, B. (1997). Regulation of Synaptic
816 Efficacy by Coincidence of Postsynaptic APs and EPSPs. *Science* 275, 213–215.
817 10.1126/science.275.5297.213.

818 10. Magee, J.C., and Johnston, D. (1997). A Synaptically Controlled, Associative Signal for
819 Hebbian Plasticity in Hippocampal Neurons. *Science* 275, 209–213.
820 10.1126/science.275.5297.209.

821 11. Bittner, K.C., Grienberger, C., Vaidya, S.P., Milstein, A.D., Macklin, J.J., Suh, J., Tonegawa,
822 S., and Magee, J.C. (2015). Conjunctive input processing drives feature selectivity in
823 hippocampal CA1 neurons. *Nat. Neurosci.* 18, 1133–1142. 10.1038/nn.4062.

824 12. Bittner, K.C., Milstein, A.D., Grienberger, C., Romani, S., and Magee, J.C. (2017).
825 Behavioral time scale synaptic plasticity underlies CA1 place fields. *Science* 357, 1033–
826 1036. 10.1126/science.aan3846.

827 13. Fan, L.Z., Kim, D.K., Jennings, J.H., Tian, H., Wang, P.Y., Ramakrishnan, C., Randles, S.,
828 Sun, Y., Thadhani, E., Kim, Y.S., et al. (2023). All-optical physiology resolves a synaptic
829 basis for behavioral timescale plasticity. *Cell* 186, 543-559.e19. 10.1016/j.cell.2022.12.035.

830 14. Milstein, A.D., Li, Y., Bittner, K.C., Grienberger, C., Soltesz, I., Magee, J.C., and Romani, S.
831 (2021). Bidirectional synaptic plasticity rapidly modifies hippocampal representations. *eLife*
832 10, e73046. 10.7554/eLife.73046.

833 15. Priestley, J.B., Bowler, J.C., Rolotti, S.V., Fusi, S., and Losonczy, A. (2022). Signatures of
834 rapid plasticity in hippocampal CA1 representations during novel experiences. *Neuron* 110,
835 1978-1992.e6. 10.1016/j.neuron.2022.03.026.

836 16. Grienberger, C., and Magee, J.C. (2022). Entorhinal cortex directs learning-related changes
837 in CA1 representations. *Nature*, 1–9. 10.1038/s41586-022-05378-6.

838 17. Allen, K., Rawlins, J.N.P., Bannerman, D.M., and Csicsvari, J. (2012). Hippocampal Place
839 Cells Can Encode Multiple Trial-Dependent Features through Rate Remapping. *J. Neurosci.*
840 32, 14752–14766. 10.1523/JNEUROSCI.6175-11.2012.

841 18. Leutgeb, S., Leutgeb, J.K., Barnes, C.A., Moser, E.I., McNaughton, B.L., and Moser, M.-B.
842 (2005). Independent Codes for Spatial and Episodic Memory in Hippocampal Neuronal
843 Ensembles. *Science* 309, 619–623. 10.1126/science.1114037.

844 19. Dong, C., Madar, A.D., and Sheffield, M.E.J. (2021). Distinct place cell dynamics in CA1 and
845 CA3 encode experience in new environments. *Nat. Commun.* 12, 2977. 10.1038/s41467-
846 021-23260-3.

847 20. Huszár, R., Zhang, Y., Blockus, H., and Buzsáki, G. (2022). Preconfigured dynamics in the
848 hippocampus are guided by embryonic birthdate and rate of neurogenesis. *Nat. Neurosci.*
849 25, 1201–1212. 10.1038/s41593-022-01138-x.

850 21. Hainmueller, T., and Bartos, M. (2018). Parallel emergence of stable and dynamic memory
851 engrams in the hippocampus. *Nature* 558, 292–296. 10.1038/s41586-018-0191-2.

852 22. Frank, L.M. (2004). Hippocampal Plasticity across Multiple Days of Exposure to Novel
853 Environments. *J. Neurosci.* 24, 7681–7689. 10.1523/jneurosci.1958-04.2004.

854 23. Sheffield, M.E.J., Adoff, M.D., and Dombeck, D.A. (2017). Increased prevalence of calcium
855 transients across the dendritic arbor during place field formation. *Neuron* 96, 490-504.e5.
856 10.1016/j.neuron.2017.09.029.

857 24. Jackson, B., Scargle, J.D., Barnes, D., Arabhi, S., Alt, A., Gioumousis, P., Gwin, E.,
858 Sangtrakulcharoen, P., Tan, L., and Tsai, T.T. (2005). An algorithm for optimal partitioning
859 of data on an interval. *IEEE Signal Process. Lett.* 12, 105–108. 10.1109/LSP.2001.838216.

860 25. Monaco, J.D., Rao, G., Roth, E.D., and Knierim, J.J. (2014). Attentive Scanning Behavior
861 Drives One-Trial Potentiation of Hippocampal Place Fields. *Nat. Neurosci.* 17, 725–731.
862 10.1038/nn.3687.

863 26. Frank, L.M., Brown, E.N., and Wilson, M. (2000). Trajectory Encoding in the Hippocampus
864 and Entorhinal Cortex. *Neuron* 27, 169–178. 10.1016/S0896-6273(00)00018-0.

865 27. Wood, E.R., Dudchenko, P.A., Robitsek, R.J., and Eichenbaum, H. (2000). Hippocampal
866 Neurons Encode Information about Different Types of Memory Episodes Occurring in the
867 Same Location. *Neuron* 27, 623–633. 10.1016/S0896-6273(00)00071-4.

868 28. Mizuseki, K., and Buzsáki, G. (2013). Preconfigured, Skewed Distribution of Firing Rates in
869 the Hippocampus and Entorhinal Cortex. *Cell Rep.* 4, 1010–1021.
870 10.1016/j.celrep.2013.07.039.

871 29. McKenzie, S., Huszár, R., English, D.F., Kim, K., Christensen, F., Yoon, E., and Buzsáki, G.
872 (2021). Preexisting hippocampal network dynamics constrain optogenetically induced place
873 fields. *Neuron* 109, 1040-1054.e7. 10.1016/j.neuron.2021.01.011.

874 30. Robinson, N.T.M., Descamps, L.A.L., Russell, L.E., Buchholz, M.O., Bicknell, B.A., Antonov,
875 G.K., Lau, J.Y.N., Nutbrown, R., Schmidt-Hieber, C., and Häusser, M. (2020). Targeted
876 Activation of Hippocampal Place Cells Drives Memory-Guided Spatial Behavior. *Cell* 183,
877 1586-1599.e10. 10.1016/j.cell.2020.09.061.

878 31. Rolotti, S.V., Ahmed, M.S., Szoboszlay, M., Geiller, T., Negrean, A., Blockus, H., Gonzalez,
879 K.C., Sparks, F.T., Canales, A.S.S., Tuttman, A.L., et al. (2022). Local feedback inhibition
880 tightly controls rapid formation of hippocampal place fields. *Neuron* 110, 783-794.e6.
881 10.1016/j.neuron.2021.12.003.

882 32. Deitch, D., Rubin, A., and Ziv, Y. (2021). Representational drift in the mouse visual cortex.
883 *Curr. Biol.* 31, 4327-4339.e6. 10.1016/j.cub.2021.07.062.

884 33. Geva, N., Deitch, D., Rubin, A., and Ziv, Y. (2023). Time and experience differentially affect
885 distinct aspects of hippocampal representational drift. *Neuron* 111.
886 10.1016/j.neuron.2023.05.005.

887 34. Khatib, D., Ratzon, A., Sellevoll, M., Barak, O., Morris, G., and Derdikman, D. (2023). Active
888 experience, not time, determines within-day representational drift in dorsal CA1. *Neuron*
889 111, 2348-2356.e5. 10.1016/j.neuron.2023.05.014.

890 35. Mankin, E.A., Sparks, F.T., Slayyeh, B., Sutherland, R.J., Leutgeb, S., and Leutgeb, J.K.
891 (2012). Neuronal code for extended time in the hippocampus. *Proc. Natl. Acad. Sci.* 109,
892 19462-19467. 10.1073/pnas.1214107109.

893 36. Rubin, A., Geva, N., Sheintuch, L., and Ziv, Y. (2015). Hippocampal ensemble dynamics
894 timestamp events in long-term memory. *eLife* 4, e12247. 10.7554/eLife.12247.

895 37. Tononi, G., and Cirelli, C. (2006). Sleep function and synaptic homeostasis. *Sleep Med.*
896 *Rev.* 10, 49–62. 10.1016/j.smrv.2005.05.002.

897 38. Watson, B.O., Levenstein, D., Greene, J.P., Gelinas, J.N., and Buzsáki, G. (2016). Network
898 Homeostasis and State Dynamics of Neocortical Sleep. *Neuron* 90, 839–852.
899 10.1016/j.neuron.2016.03.036.

900 39. deCharms, R.C., and Zador, A. (2000). Neural Representation and the Cortical Code. *Annu.*
901 *Rev. Neurosci.* 23, 613–647. 10.1146/annurev.neuro.23.1.613.

902 40. Fenton, A.A., Lytton, W.W., Barry, J.M., Lenck-Santini, P.P., Zinyuk, L.E., Kubik, S., Bures,
903 J., Poucet, B., Muller, R.U., and Olypher, A.V. (2010). Attention-Like Modulation of
904 Hippocampus Place Cell Discharge. *J. Neurosci.* 30, 4613–4625. 10.1523/jneurosci.5576-
905 09.2010.

906 41. Fenton, A.A., and Muller, R.U. (1998). Place cell discharge is extremely variable during
907 individual passes of the rat through the firing field. *Proc. Natl. Acad. Sci.* 95, 3182–3187.
908 10.1073/pnas.95.6.3182.

909 42. Jackson, J., and Redish, A.D. (2007). Network dynamics of hippocampal cell-assemblies
910 resemble multiple spatial maps within single tasks. *Hippocampus* 17, 1209–1229.
911 10.1002/hipo.20359.

912 43. Kentros, C.G., Agnihotri, N.T., Streater, S., Hawkins, R.D., and Kandel, E.R. (2004).
913 Increased Attention to Spatial Context Increases Both Place Field Stability and Spatial
914 Memory. *Neuron* 42, 283–295. 10.1016/s0896-6273(04)00192-8.

915 44. Pettit, N.L., Yuan, X.C., and Harvey, C.D. (2022). Hippocampal place codes are gated by
916 behavioral engagement. *Nat. Neurosci.* 25, 561–566. 10.1038/s41593-022-01050-4.

917 45. Sadeh, S., and Clopath, C. (2022). Contribution of behavioural variability to representational
918 drift. *eLife* 11, e77907. 10.7554/eLife.77907.

919 46. Zemla, R., Moore, J.J., Hopkins, M.D., and Basu, J. (2022). Task-selective place cells show
920 behaviorally driven dynamics during learning and stability during memory recall. *Cell Rep.*
921 41, 111700. 10.1016/j.celrep.2022.111700.

922 47. Harvey, C.D., Coen, P., and Tank, D.W. (2012). Choice-specific sequences in parietal
923 cortex during a virtual-navigation decision task. *Nature* 484, 62–68. 10.1038/nature10918.

924 48. Pastalkova, E., Itskov, V., Amarasingham, A., and Buzsáki, G. (2008). Internally Generated
925 Cell Assembly Sequences in the Rat Hippocampus. *Science* 321, 1322–1327.
926 10.1126/science.1159775.

927 49. Kispesky, T., White, J.A., and Rotstein, H.G. (2010). The Mechanism of Abrupt Transition
928 between Theta and Hyper-Excitable Spiking Activity in Medial Entorhinal Cortex Layer II
929 Stellate Cells. *PLOS ONE* 5, e13697. 10.1371/journal.pone.0013697.

930 50. Dragoi, G., Harris, K.D., and Buzsáki, G. (2003). Place Representation within Hippocampal
931 Networks Is Modified by Long-Term Potentiation. *Neuron* 39, 843–853. 10.1016/S0896-
932 6273(03)00465-3.

933 51. Royer, S., and Paré, D. (2003). Conservation of total synaptic weight through balanced
934 synaptic depression and potentiation. *Nature* 422, 518–522. 10.1038/nature01530.

935 52. Geiller, T., Sadeh, S., Rolotti, S.V., Blockus, H., Vancura, B., Negrean, A., Murray, A.J.,
936 Rózsa, B., Polleux, F., Clopath, C., et al. (2022). Local circuit amplification of spatial
937 selectivity in the hippocampus. *Nature* 601, 105–109. 10.1038/s41586-021-04169-9.

938 53. Lee, D., Lin, B.-J., and Lee, A.K. (2012). Hippocampal Place Fields Emerge upon Single-
939 Cell Manipulation of Excitability During Behavior. *Science* 337, 849–853.
940 10.1126/science.1221489.

941 54. Valero, M., Zutshi, I., Yoon, E., and Buzsáki, G. (2022). Probing subthreshold dynamics of
942 hippocampal neurons by pulsed optogenetics. *Science* 375, 570–574.
943 10.1126/science.abm1891.

944 55. Truong, C., Oudre, L., and Vayatis, N. (2020). Selective review of offline change point
945 detection methods. *Signal Process.* 167, 107299. 10.1016/j.sigpro.2019.107299.

946 56. Seabold, S., and Perktold, J. (2010). Statsmodels: Econometric and Statistical Modeling
947 with Python. In, pp. 92–96. 10.25080/Majora-92bf1922-011.

948

949

950

951

952

953

954

955

956

957

958

959

960

961

962

963

964

965

966

967

968